NASA Technical Memorandum 83125

NASA-TM-83125 19810016800

INTEGRATED TRANSIENT THERMAL-STRUCTURAL FINITE ELEMENT ANALYSIS

EARL A. THORNTON, PRAMOTE DECHAUMPHAI,
ALLAN R. WIETING, AND KUMAR K. TAMMA

MAY 1981

National Aeronautics and
Space Administration

Langley Research Center
Hampton, Virginia 23665

INTEGRATED TRANSIENT THERMAL-STRUCTURAL FINITE ELEMENT ANALYSIS

Earl A. Thornton* and Pramote Dechaumphai**
Old Dominion University
Norfolk, Virginia

Allan R. Wieting***
NASA Langley Research Center
Hampton, Virginia

and

Kumar K. Tamma**
Old Dominion University
Norfolk, Virginia

Abstract

An integrated thermal-structural finite element approach for efficient coupling of transient thermal and structural analysis is presented. New integrated thermal-structural rod and one dimensional axisymmetric elements considering conduction and convection are developed and used in transient thermal-structural applications. The improved accuracy of the integrated approach is illustrated by comparisons with exact transient heat conduction-elasticity solutions and conventional finite element thermal-finite element structural analyses. Results indicate that the approach offers significant potential for further development with other elements.

Nomenclature

a	inner radius of cylinder, see fig. 4
A	cross-sectional area
b	outer radius of cylinder, see fig. 4
$[B_S]$	strain-displacement interpolation matrix
$[B_T]$	temperature gradient interpolation matrix
c	specific heat
c_i	arbitrary constants, see equation (8)
$[C]$	finite element capacitance matrix
$[D]$	elasticity matrix
$f(x)$	forcing function, see equation (7)
$f_i(x)$	homogeneous solution, see equation (8)
$g(x)$	particular solution, see equation (8)
E	modulus of elasticity
F	force
$\{F\}_e$	finite element nodal force vector
h	convective heat transfer coefficient
k	thermal conductivity
$[k]_e$	thermal conductivity matrix
$[K]_e$	finite element stiffness matrix
$[K_c]_e$	finite element conductance matrix for conduction
$[K_h]_e$	finite element conductance matrix for convection
L	length
m	conduction-convection rod parameter, $m = \sqrt{hp/kA}$
n	order of differential equation, see equation (7)
$N_o(x)$	finite element interpolation function for nodeless variables, see equation (10)
$[N]$	finite element interpolation functions
$[N_S]$	finite element displacement interpolation functions
$[N_T]$	finite element temperature interpolation functions
p	perimeter
q	surface heating rates
r	radial coordinate, see fig. 4
Q	volumetric heat generation rate
$\{Q\}_e$	finite element heat load vector
S_e	finite element surface area
t	time
T	temperature
T_o	nodeless parameter
$T_o(t)$	nodeless variable
T_r	reference temperature for zero stress
T_∞	environmental temperature for convective heat exchange
u,v,w	displacement components
w	$\ln(b/a)$, see table 4
V_e	finite element volume
x,y,z	cartesian coordinates
X	nondimensional coordinate, $X = x/L$
$\{\alpha\}$	vector of thermal expansion coefficients
ρ	density
$\phi(x)$	dependent variable in differential equation, see equation (7)

Subscripts

c	conduction heat transfer
e	element matrix or vector
h	convective heat transfer
S	structural
T	thermal

Superscript

T	transpose of a matrix

Introduction

A recent overview[1] of research in structures and materials for future space transportation systems cited the challenge of providing lightweight structures for large space transportation vehicles that are repeatedly subjected to severe aerodynamic heating and yet

*Associate Professor, Mechanical Engineering and Mechanics Department
**Research Assistant, Mechanical Engineering and Mechanics Department
***Head, Aerothermal Loads Branch, Loads and Aeroelasticity Division

must have structural efficiency, reliability and durability approaching that of commercial aircraft. One of the most challenging thermal-structural analyses faced by aerospace engineers today is the Space Shuttle Orbiter. Shuttle design experience has shown that the design of large structures for hostile reentry environment taxes the capability of existing thermal and structural analysis methods. The complex thermal behavior of the Shuttle has required a large number of highly detailed lumped parameter analytical models. A review[2] of needs revealed by the Shuttle thermal analysis cited the need for improved modeling procedures to reduce model size and more efficient methods of transferring data between thermal and structural models. Experience in the repetitious thermal and structural analyses required for the design of convectively-cooled structures and in the optimum design[3] of structures subjected to heating and mechanical loads at elevated temperatures also points to the need for more efficient coupling of the thermal and structural analyses.

Thermal analysis of complex structures is generally carried out by one of two alternative methods: (1) the finite difference lumped parameter method, or (2) the finite element method. The lumped parameter approach is most widely used, but the finite element method is an attractive alternative since it provides capabilities for both thermal and structural analysis of general structures. Frequently the thermal analysis is performed by the lumped parameter method and the structural analysis by the finite element method. Because of basic differences between the analytical models an efficient interface is difficult to achieve.

The finite element method offers the greatest potential for efficient coupling of the thermal and structural analyses, but the historically better capabilities and efficiency of the lumped parameter method compared to early finite element methods has so far prevented the finite element method from receiving widespread acceptance for thermal analysis. Recent experience[4] with the finite element method for combined conduction forced convection analysis has shown that: (1) the methods currently have about the same analysis capabilities, (2) the finite element method has superior accuracy, and (3) the lumped parameter method maintains an edge in efficiency, but that as additional finite element experience is gained, improvements in efficiency can be achieved.

Research programs are currently underway at Langley Research Center to improve both the capabilities and efficiency of the finite element thermal analysis method and develop more efficient coupling between the finite element thermal and structural analyses. The authors previously presented a paper[5] which focused on finite element methodology for efficient coupling of steady-state thermal and structural analyses. The purpose of this paper is to extend the methodology, denoted as integrated thermal-structural analysis, for the transient-thermal static-structural analysis case.

Characteristics of integrated thermal-structural analysis are first discussed. A nodeless variable approach for the development of transient integrated thermal-structural elements is then described. Next, the nodeless variable approach is used to develop new integrated thermal-structural rod and one-dimensional axisymmetric elements. Finally, the accuracy and efficiency of the integrated approach is demonstrated by solving three thermal-structural examples by both the conventional and integrated finite element approaches. In two of the examples, the accuracy of the finite element solutions is evaluated by comparisons with exact transient heat conduction-elasticity solutions. Finite element matrices are presented in Appendices.

Integrated Thermal-Structural Analysis

Finite Element Analysis

Finite element (F.E.) formulations for transient thermal problems are derived by the method of weighted residuals.[6] In general, element temperature $T(x,y,z,t)$ and temperature gradients are expressed in the form

$$\{T\} = [N_T]\{T(t)\}_e \tag{1a}$$

$$\begin{Bmatrix} \partial T/\partial x \\ \partial T/\partial y \\ \partial T/\partial z \end{Bmatrix} = [B_T]\{T\}_e \tag{1b}$$

where $[N_T]$ denotes a matrix of the temperature interpolation functions, $[B_T]$ denotes a matrix of temperature gradient interpolation functions and $\{T(t)\}_e$ denotes a vector (one dimensional array) of nodal temperatures. For transient thermal analysis of conduction with convection boundary conditions the equations for a typical element are

$$[C]_e\{\dot{T}\}_e + [K_c + K_h]_e\{T\}_e = \{Q\}_e \tag{2}$$

where $[C]_e$ is the element capacitance matrix, $[K_c]_e$ and $[K_h]_e$ are element conduction and convection conductance matrices, respectively, and $\{Q\}_e$ is a vector of nodal heat loads. These matrices, in general, are expressed in the form of integrals over the volume, V_e, and surface, S_e, of an element. The element equations are

$$[C]_e = \int_{V_e} \rho c[N_T]^T[N_T]dV \tag{3a}$$

$$[K_c]_e = \int_{V_e} [B_T]^T[k][B_T]dV \tag{3b}$$

$$[K_h]_e = \int_{S_e} h[N_T]^T[N_T]dS \tag{3c}$$

$$\{Q\}_e = \int_{V_e} Q[N_T]^T dV + \int_{S_e} q[N_T]^T dS + \int_{S_e} h\, T_\infty [N_T]^T dS \tag{3d}$$

where ρ is the density, c is the specific heat, $[k]$ denotes the conductivity matrix, h is a convection coefficient, Q is an internal heat generation rate per unit volume, q is a surface heating rate per unit area and T_∞ denotes the environmental temperature for the convective heat exchange. The superscript T denotes the transpose of a matrix. The convection coefficient, the internal heat generation rate, the surface heating rate and the environmental temperature are, in

general, time-dependent. All thermal parameters, herein, are assumed constant although they may be temperature dependent in general. Finite element formulations for other heat transfer modes such as forced convection and radiation are given in references 4 and 7, respectively. The simultaneous differential equations (2) are typically solved by time-marching schemes so that the temperatures {T} are computed at discrete time values.

In general formulations of transient thermal-stress problems, the heat transfer and elasticity solutions are coupled through a mechanical coupling term in the heat conduction equation and inertia terms in the elasticity equations. In most engineering applications the coupling effects are not significant, and the coupling terms are neglected. In the uncoupled formulation, transient temperatures are computed in the thermal analysis and are used as input to a quasi-static structural analysis. Finite element formulations for the structural analysis are usually derived from a variational formulation.[6] Since the structural temperatures vary with time, the structural analysis consists of a sequence of static analyses at selected time values in the transient thermal analysis. In a typical structural analysis, element displacements (u,v,w) are expressed in the form

$$\{u\} = [N_S]\{u\}_e \tag{4}$$

where $[N_S(x,y,z)]$ denotes the displacement interpolation functions, and $\{u\}_e$ denotes a vector of element nodal displacements. For the structural analysis the equations for a typical element are

$$[K]_e\{u\}_e = \{F\}_e \tag{5}$$

where $[K]_e$ is the element stiffness matrix, and $\{F\}$ is a vector of nodal forces which can consist of mechanical forces and/or equivalent thermal forces. Only the equations for the equivalent thermal force will be shown herein. The element equations are

$$[K]_e = \int_{V_e} [B_S]^T [D][B_S]dV \tag{6a}$$

$$\{F\}_e = \int_{V_e} [B_S]^T [D]\{\alpha\}T\, dV \tag{6b}$$

where $[B_S]$ is the strain-displacement interpolation matrix, $[D]$ denotes the elasticity matrix, and $\{\alpha\}$ is a vector of thermal expansion coefficients. $T(x,y,z,t)$ is the temperature within the element computed in the transient thermal analysis.

The temperatures enter the structural analysis in two ways: (1) the structural elasticity matrix $[D]$ and thermal expansion coefficient vector $\{\alpha\}$ are, in general, temperature dependent, and (2) the equivalent thermal forces, equation (6b), involves an integration of the temperature $T(x,y,z,t)$ over the element volume. For a temperature dependent elasticity matrix, the element stiffness matrix, equation (6a), varies during the transient response. In this paper the elastic properties and the thermal expansion coefficient are assumed constant, hence the element stiffness matrix is constant and is computed only once. The nodal forcevector is computed for each temperature vector at the selected time values, and consequently the structural analysis is a static analysis with multiple load cases.

Integrated Analysis

A step toward integrated thermal-structural analysis capability is the use of a common methodology in a single program such as NASTRAN[8] which contains both thermal and structural analysis capability. One disadvantage of this approach, herein called the conventional approach, is that the transfer of data between analyses is often inefficient because of inherent differences between the thermal and structural models. Another disadvantage of the conventional approach is that basic differences between the thermal and structural analysis requirements are not recognized and exploited. For example, the very common beam, plate and shell structural finite elements have no thermal counterparts in typical finite element thermal analysis programs because conventional finite elements have no provision for computing thickness-temperature gradients. This deficiency means not only that the thermal and structural finite element models of the same structure differ, but that thermal load data (e.g. temperature gradients) are not directly supplied by the thermal analysis.

To exploit more fully the capabilities of the F.E. method the concept of integrated thermal-structural analysis was proposed in reference 5. An integrated thermal structural analysis is characterized by: (1) thermal and structural finite elements formulated with a common geometric discretization with each element formulated to suit the needs of their respective analysis, (2) thermal and structural finite elements which are fully compatible, and (3) equivalent thermal forces which are based upon the consistent finite element force vector computed by equation (6b).

The concepts of conventional and integrated thermal-structural analysis approaches are compared schematically in Fig. 1. The sequence followed in a conventional analysis is shown in Fig. 1(a). First, a thermal analysis is performed based upon a thermal model selected to best represent the heat transfer problem. The thermal model may be based on the lumped parameter or F.E. method. The thermal analysis is followed by transfer of the nodal temperature data to the structural analysis. In most cases this data transfer involves data processing to bring the input temperatures in conformity with the needs of the structural model. Often the structural and thermal models use different nodes and elements, and approximate thermal forces are computed from average element temperatures. An integrated analysis is shown in Fig. 1(b). The thermal and structural analyses are characterized by a common model based upon thermal and structural elements formulated to best suit the respective analysis. The transfer of data is compatible with no data processing required. Consistent thermal forces are computed from thermal elemental and nodal input data supplied directly from the thermal analysis.

Integrated Elements

The concept of integrated transient thermal-structural analysis is illustrated with a new rod element and a new one-dimensional axisymmetric element based on nodeless variable formulations. The one-dimensional integrated elements consider combined conduction and

convection with constant thermal parameters. The nodeless variable approach[6] was utilized in reference 5 to develop an integrated rod element for steady state analysis. The nodeless variable approach as used herein consists of utilizing improved temperature interpolation functions which employ an element or "nodeless" variable. The nodeless variable approach has been used previously in structural analysis by adding extra interpolation functions (sometimes called "bubble" modes) to the conventional interpolation functions. A unique feature of the nodeless variable approach for steady state analysis is the use of an exact temperature variation to compute the element conductance matrices, heat load vectors and equivalent thermal forces. The exact temperature variation is also used to compute an exact displacement variation in the structural element.

Exact Steady-State Formulation

Finite elements which yield exact values of the nodal variables will herein be called exact finite elements. Structural rod and beam elements under simple loadings are known to produce exact values of the nodal displacements. Linear conduction elements under simple heating also produce exact values of nodal temperatures.[6] Further, in one-dimensional combined conduction-forced convection heat transfer an exact F.E. has been derived[9] using the Galerkin method with upwind weighting functions. In this section an approach[5] for deriving exact finite elements in one-dimensional problems will be described. The approach is based upon using the exact solution to the corresponding linear, steady-state differential equation to derive the element interpolation functions. If the elements are used alone (i.e. without connections to other element families) an exact solution will be obtained. Approximate solutions will be obtained if the elements are used in transient or nonlinear applications, or if the elements are connected to elements of other non-exact interpolation function families.

Consider a linear, nonhomogeneous differential equation

$$a_n \, d^n\phi/dx^n + a_{n-1} \, d^{n-1}\phi/dx^{n-1} + \ldots + a_0\phi = f(x) \tag{7}$$

where $\phi(x)$ is the dependent variable. The exact solution has the form

$$\phi(x) = \sum_{i=1}^{n} c_i f_i(x) + g(x) \tag{8}$$

where c_i are arbitrary constants, $f_i(x)$ are typical functions in the homogeneous solution, and $g(x)$ is the particular solution. A F.E. with n degrees of freedom is formulated based upon the continuity requirements for nodal variables.[10] For example, if the dependent variable only is required to be continuous at element nodes then an element with n nodes will permit an exact solution. Since the differential equation has n constants of integration the element interpolation functions are determined by imposing the conditions

$$\phi(x_i) = \phi_i \qquad i = 1,2,\ldots,n \tag{9}$$

where x_i are the nodal coordinates, and ϕ_i are the nodal values of the dependent variables. To accommodate the particular solution, $g(x)$, the element interpolation function is written in the form

$$\phi(x) = N_o(x)\phi_o + \sum_{i=1}^{n} N_i(x)\phi_i \tag{10}$$

where ϕ_o is a nodeless variable.[6] In applications ϕ_o is selected as a convenient parameter and consequently is a known quantity a priori. Note that since $N_i(x_i) = 1$ to satisfy eq. (9), then $N_o(x_i) = 0$. With the exact interpolation functions known, the element matrices can be derived using typical finite element integrals such as eqs. (3) for thermal analysis or eqs. (6) for structural analysis. Element matrices are generally of size n + 1 due to the presence of the nodeless variable. In many cases (see Appendices A and B) the extra equation is uncoupled so that in the computer analysis only matrices of size n are employed.

Transient Formulation

In Ref. 5, the nodeless approach was used to develop an exact integrated thermal-structural rod element for steady-state conduction and convection analysis. One dimensional elements such as the rod element are characterized by two nodal unknowns and one nodeless variable for the steady-state thermal or structural element formulations where the nodeless variable is identified as a convenient physical parameter and is known for each element.

For general transient analysis it is not possible to formulate closed-form interpolation functions which are exact solutions since general transient solutions to the heat conduction-elasticity equations are infinite series. However, the nodeless variable interpolation function concept introduced in eq. (10) can be extended for the transient case to give accuracy superior to the conventional finite element approach. To extend the nodeless variable approach to the transient case, two approaches are investigated: (1) the nodeless variable approach previously described for steady-state analysis, which hereafter is referred to as the nodeless parameter formulation, and (2) a nodeless variable approach where the nodeless variable is an unknown function of time.

Nodeless parameter approach. In the nodeless parameter approach the temperature interpolation, eq. (10), for an element with two nodes has the form

$$T(x,t) = N_o(x)T_o + N_1(x)\,T_1(t) + N_2(x)\,T_2(t) \tag{11}$$

where T_o is a known nodeless parameter, and $T_1(t)$, $T_2(t)$ are unknown time-dependent nodal temperatures. The element equations, eq. (2), for a typical element based on this approach may be written as

$$\begin{bmatrix} C_{00} & C_{01} & C_{02} \\ C_{10} & C_{11} & C_{12} \\ C_{20} & C_{21} & C_{22} \end{bmatrix} \begin{Bmatrix} 0 \\ \dot{T}_1 \\ \dot{T}_2 \end{Bmatrix} + \begin{bmatrix} K_{00} & 0 & 0 \\ 0 & K_{11} & K_{12} \\ 0 & K_{21} & K_{22} \end{bmatrix} \begin{Bmatrix} T_0 \\ T_1 \\ T_2 \end{Bmatrix} = \begin{Bmatrix} Q_0 \\ Q_1 \\ Q_2 \end{Bmatrix} \quad (12)$$

where the element subscript e has been omitted. The salient characteristic of this element formulation is that the first equation involving the nodeless parameter is uncoupled from the nodal unknowns in the second and third equations. Thus the element matrices have two unknowns as for a conventional element.

Nodeless variable approach. In the nodeless variable approach the temperature interpolation, eq. (10), for an element with two nodes has the form

$$T(x,t) = N_0(x)\, T_0(t) + N_1(x)\, T_1(t) + N_2(x)\, T_2(t) \quad (13)$$

where $T_0(t)$ is an unknown time-dependent nodeless variable, and $T_1(t)$, $T_2(t)$ are unknown time-dependent nodal temperatures. Note that for steady-state solutions the nodeless variable has a value equal to T_0. The element equations, eq. (2), for a typical element now have the form

$$\begin{bmatrix} C_{00} & C_{01} & C_{02} \\ C_{10} & C_{11} & C_{12} \\ C_{20} & C_{21} & C_{22} \end{bmatrix} \begin{Bmatrix} \dot{T}_0 \\ \dot{T}_1 \\ \dot{T}_2 \end{Bmatrix} + \begin{bmatrix} K_{00} & 0 & 0 \\ 0 & K_{11} & K_{12} \\ 0 & K_{21} & K_{22} \end{bmatrix} \begin{Bmatrix} T_0 \\ T_1 \\ T_2 \end{Bmatrix} = \begin{Bmatrix} Q_0 \\ Q_1 \\ Q_2 \end{Bmatrix} \quad (14)$$

Since the nodeless variable is unknown, the equations are coupled through the capacitance matrix due to the presence of $\dot{T}_0$. Thus the element matrices have three unknowns, one more degree of freedom than a conventional element.

A unique feature of the nodeless parameter and nodeless variable interpolation equations is that in the steady-state each reduce to the exact solution. This means the transient response can start from an exact initial temperature distribution and also as time becomes large, the transient response will approach an exact steady-state solution. A unique feature of the temperature interpolation presented in equation (13) is that the temperature interpolation within an element is time dependent. Typical behavior of conventional, nodeless parameter and nodeless variable interpolation functions during a transient response are compared in Fig. 2. The figure shows that the conventional and nodeless parameter temperature interpolations retain the same shape during the response, but the amplitude of the nodeless variable temperature interpolation varies throughout the response.

Rod Element

Characteristics of the thermal and structural models of a rod element are shown in Fig. 3. Four heat transfer cases (Table 1) are considered in the thermal model with axial conduction combined with internal heat generation (source or sink), surface heat flux or surface convection. For transient heat transfer, an energy balance on a small segment of the rod gives the governing differential equations for the temperature distribution, T(x,t):

$$-kA \frac{\partial^2 T}{\partial x^2} + \rho cA \frac{\partial T}{\partial t} = 0 \quad \text{(Case 1)} \quad (15a)$$

$$-kA \frac{\partial^2 T}{\partial x^2} + \rho cA \frac{\partial T}{\partial t} = QA \quad \text{(Case 2)} \quad (15b)$$

$$-kA \frac{\partial^2 T}{\partial x^2} + \rho cA \frac{\partial T}{\partial t} = qp \quad \text{(Case 3)} \quad (15c)$$

$$-kA \frac{\partial^2 T}{\partial x^2} + \rho cA \frac{\partial T}{\partial t} + hpT = hpT_\infty \quad \text{(Case 4)} \quad (15d)$$

where A is the element cross-sectional area and p is the perimeter. The temperature interpolation functions are first derived by solving for steady-state solutions to the differential equations above. The nodeless parameters and exact temperature interpolation functions are then written in the form of equation (10); the results are shown in Table 2. For Case 1 the results are the same as the conventional F.E.; linear interpolation functions yield the exact solution. For Cases 2-3, the results are modified by the $N_0(x)$ term which introduces a parabolic variation of temperature from the nonhomogeneous terms, the heat loads. For Case 4, a completely new form for the interpolation function is obtained which heat transfer analysts recognize as the solution for a fin with prescribed end temperatures.

The exact temperature interpolation functions (Table 2) are used to derive the element capacitance and conductance matrices and heat load vectors by evaluating the integral definitions given in equation (3); the results are presented in Appendix A.

Use of the exact rod element interpolation functions (Table 2) and the element matrices yield exact steady-state rod temperatures, but the full benefit of the results is not realized unless incorporated consistently in the structural analysis.

For the structural response a force balance on a small segment of the rod (Fig. 2) gives the governing differential equation for the member axial displacement, u(x,t)

$$EA\, \partial^2 u/\partial x^2 = \alpha EA\, \partial T/\partial x \quad (16)$$

where E is the modulus of elasticity and α is the coefficient of thermal expansion. In the conventional two node structural element the displacement varies linearly and yields an exact stiffness matrix. For mechanical loads applied at the nodes, exact nodal displacements are obtained. Yet, in conventional thermal-structural analysis a linear variation of temperature is assumed in computing the thermal forces from equation (6b). Since a linear variation is an approximation to the true temperature distribution for Cases 2-4, only approximate thermal forces are obtained thereby reducing the accuracy of the structural analysis.

In the integrated thermal-structural analysis the temperatures (Eq. 10 and Table 2) are employed to derive a consistent set of thermal forces. First, the temperature interpolation functions given in Table 2 are differentiated and substituted into the right-hand side of Eq. (16) and the differential equations are solved. The

exact displacement interpolation functions are derived in the form of Eq. (10) and are shown in Table 3. The results for $N_1(x)$ and $N_2(x)$ are the same for all four cases and are the conventional linear interpolation functions. The conventional linear temperature distribution is modified by the $N_0(x)$ term yielding in each case a nonlinear displacement variation within the element. The nonlinear variation depends on the element nodal temperatures and hence the thermal loading.

The exact temperature interpolation functions (Table 2) and the exact displacement interpolation functions (Table 3) are used to derive the element stiffness matrices and equivalent nodal forces by evaluating the integral definitions given in equation (6); the results are presented in Appendix A.

The element stiffness matrix is the same as for conventional elements, but the force vectors differ from the conventional forces. These nodal forces, when computed using the exact nodal temperatures from the thermal analysis, will give exact nodal displacements for all heat load cases considered in contrast to the conventional approach which gives exact nodal displacements only for Case 1. Values for displacements within an element may also be computed if desired using Eq. (10) and the interpolation functions given in Table 3.

Axisymmetric Element

Characteristics of the thermal and structural models of a one dimensional axisymmetric element are shown in Fig. 4. The thermal model considers radial conduction combined with internal heat generation. Specified surface heating or surface convection on the inner and outer cylinder surfaces are considered through the boundary conditions. The governing differential equations[11] for the temperature T(r,t) are

$$-k \frac{1}{r} \frac{\partial}{\partial r} \left(r \frac{\partial T}{\partial r}\right) + \rho c \frac{\partial T}{\partial t} = 0 \quad \text{(Case 1)} \qquad (17a)$$

$$-k \frac{1}{r} \frac{\partial}{\partial r} \left(r \frac{\partial T}{\partial r}\right) + \rho c \frac{\partial T}{\partial t} = Q \quad \text{(Case 2)} \qquad (17b)$$

The corresponding nodeless parameters and element interpolation functions are derived as described previously and are shown in Table 4. For both cases the logarithmic temperature interpolation functions differ significantly from conventional linear interpolation functions. For surface boundary conditions of specified heating or convection the same interpolation functions produce exact steady-state temperature distributions. Element conductance and capacitance matrices and heat load vectors for Cases 1 and 2 and surface boundary conditions are presented in Appendix B.

For the structural response, a two-dimensional plane stress or plane strain elasticity model is assumed (Fig. 4). For plane stress the governing differential equation[12] for the radial displacement u(r,t) is

$$\frac{\partial}{\partial r}\left[\frac{1}{r}\frac{\partial (ru)}{\partial r}\right] = \alpha (1+\nu) \frac{\partial T}{\partial r} \qquad (18)$$

where ν is Poisson's ratio. The formulation of the plane strain problem is mathematically analagous; therefore, only the equations for the plane stress formulation are presented herein. The corresponding equations for plane strain may be obtained by substituting equivalent elastic constants[12] for E, ν and α. The temperature gradient interpolation functions (Table 4) are substituted into the right-hand side of Eq. 18, then the differential equations are solved and written in the form of Eq. (10). The element displacement interpolation functions are shown in Table 5 written in terms of the nodeless parameter T_0. The element stiffness matrix and equivalent nodal forces are presented in Appendix B.

For the steady-state case, the element stiffness matrix and the load vector computed using the exact temperature solution produce exact nodal displacements. Values of the displacements and stresses computed within the element are also exact. In contrast, conventional axisymmetric elements predict approximate element displacements and stresses. Moreover, such conventional elements typically predict stresses with lower accuracy than displacements. For the transient case, the integrated axisymmetric element predicts approximate displacements and stresses due to errors in the transient temperatures. Conventional elements also predict approximate transient displacements and stresses but with loss of accuracy due to temperature errors and the approximate formulation of the structural element.

Thermal-Structural Analysis Programs

The computer programs used to evaluate the integrated transient thermal-structural analysis approach are briefly described.

TAP-STAP

Integrated finite element thermal and finite element structural analysis is performed by linking TAP3 and STAP. TAP3 is an exploratory thermal analysis program similar to an earlier program TAP2[13] for steady-state and transient thermal analysis of convectively cooled structures. TAP3 is currently being used to develop thermal element methodology for integrated thermal-structural analysis. STAP[14] is an educational finite element program which was modified for this study to include the integrated rod and axisymmetric structural elements. TAP3 and STAP are linked through common mass storage files. For the rod element, element forces per $E\alpha$ are transmitted from TAP3 to STAP. For the axisymmetric element, element nodeless variables and nodal temperatures are transmitted from TAP3 to STAP.

SPAR

SPAR[15,16] a general purpose finite element program developed for production-type structural analysis and recently extended for thermal analysis was used for the conventional thermal-structural analyses. The SPAR program consists of processors which communicate through a data base to perform basic analysis tasks as shown schematically in Fig. 1(b). The incorporation of integrated thermal-structural elements into SPAR would yield a fully integrated thermal-structural analysis capability as depicted in Fig. 1(b).

Applications

The integrated thermal-structural elements are applied to three transient examples of increasing complexity: (1) a rod with surface convection, (2) a cylinder with internal heating, and (3) a wind tunnel ceramic nozzle insert. The applications demonstrate relative performance of conventional and integrated finite elements. In addition, applications (1) and (3) compare finite element solutions with exact analytical solutions. All transient finite element temperature computations are made with implicit time-marching algorithms.

Rod with Surface Convection

A rod with surface convection and specified end temperatures is shown in Fig. 5a. Initially the rod is in thermal equilibrium being cooled by convection to a medium with T_∞ = 255 K, but at $t = 0^+$ the convective exchange temperature is raised instantaneously to T_∞ = 589 K thereafter heating the rod. A thermal transient ensues with the rod temperature approaching a new equilibrium state for large time values. Rod temperatures are computed from: (1) the exact analytical solution to equation 15d, (2) a conventional finite element model, (3) the nodeless parameter approach based on equation (11), and (4) the nodeless variable approach based on equation (13). In each finite element analysis two equal-length elements were used yielding an unknown at the center of the rod. Temperature distributions for t = 0, 0.01 and 0.3 s are shown in Fig. (5b-5d).

At t = 0, Fig. 5b, the nodeless parameter and nodeless variable approach predict the exact steady-state temperature distributions indicated by the solid line. The conventional finite element predicts the center nodal temperature well, but the nonlinear rod temperature distribution is only approximated by the linear temperature distribution of the conventional element. At t = 0.01 s, Fig. 5c, typical differences in the transient temperature distributions predicted by the three finite element approaches are demonstrated clearly. The conventional element yields a fair approximation to the center temperature, but only crudely approximates the true temperature distribution. The nodeless parameter element also yields a fair approximation to the center temperature, but predicts an extremely poor temperature distribution elsewhere. The nodeless variable approach gives the best approximation for the center temperature and an excellent representation for the rod temperature distribution. As the rod temperatures approach a new steady-state distribution at t = 0.3 s (Fig. 5d) the conventional element yields a fair approximation to the center temperature and crudely approximates the temperature distribution. The nodeless parameter and nodeless variable solutions give excellent approximations for the center temperature and the entire temperature distribution at this time.

The performance of the nodeless parameter solutions at t = 0.01 s (Fig. 5b) is typical of the behavior of this approach at other intermediate times (not shown). The nodeless parameter approach employs a steady-state temperature distribution to approximate the transient behavior. Each element takes on a steady-state temperature distribution as indicated by the humps in the predicted temperatures in Fig. 5b. These results are clearly not acceptable, and therefore this approach should not be used for transient response predictions. Instead, the nodeless variable approach should be employed since it gives accuracy superior to the conventional element throughout the response and predicts exact steady-state distributions.

The use of the nodeless variable predicted temperatures in the corresponding structures problem produces more accurate displacement and stress distributions than conventional finite elements.[5] For brevity, structural calculations with the rod element are omitted herein. The benefits of the integrated thermal structural analysis are clearly demonstrated in the following two examples with the axisymmetric element.

Cylinder with Internal Heating

The cross-section of an infinite cylinder with axisymmetric internal heating and equal specified surface temperatures is shown in Fig. 6a. Initially the cylinder is in thermal equilibrium being internally heated by uniform internal heat generation Q_0 over one-half the wall thickness. At t = 0+, the internal heating is reduced to zero, and a thermal transient ensues with the cylinder temperatures decaying to a uniform distribution for large time values. The problem is a rough approximation to a cylinder made from a semi-transparent material subject to intense internal radiation.[17]

Cylinder temperature distributions are computed from: (1) a conventional finite element thermal model employing twenty uniformly spaced solid elements,and (2) a nodeless variable finite element thermal model with two equal-length axisymmetric elements. Fig. 6b shows the computed temperatures at t = 0, 100 and 1000 s. At t = 0, the two nodeless variable elements predict the exact temperature distribution, and the comparison indicates the twenty element conventional model is sufficiently refined to represent the exact solution with negligible error. For the two subsequent times in the transient response, the temperatures are in excellent agreement indicating the capability of the nodeless variable approach to predict accurate temperatures with a smaller number of elements than the conventional approach.

Transient displacements and stresses are computed from conventional and integrated structural models corresponding to the previous thermal models and a conventional finite element structural model with two equal-length solid elements. Figs. 6b-6c show the computed displacements and stresses, respectively, at times corresponding to the thermal analysis. At t = 0, exact displacements and stresses are predicted by the two integrated elements, and the validity of the twenty element conventional structural model, is verified by comparison with the exact solution. For the two subsequent times in the transient analysis, the two element nodeless variable approach yields excellent agreement with the displacements and stresses from the refined conventional element model demonstrating the

effectiveness of the integrated thermal-structural analysis technique.

The importance of integrating the thermal and structural analysis is demonstrated by the results from the two element structural model shown in Figs. 6b-6c. This model predicts displacements and stresses consistently too low and is inadequate to represent the structural response. The significant point demonstrated by the analysis is that even though the correct nodal temperatures were employed, the conventional two element model was inadequate to represent the structural response because the element thermal forces are computed from a linear temperature variation which is a poor approximation for the actual temperatures, and the conventional two element structural model was inadequate to represent the cylinder stiffness. Thus for improved thermal-structural analysis it is not sufficient to use nodal temperatures from a more accurate temperature calculation; the structural model must be consistently formulated to effectively utilize the improved temperature distribution and correctly model the structural stiffness.

Wind Tunnel Nozzle Insert

In a recent paper[18] ceramic nozzle inserts (Fig. 7a) for the Langley 8-Foot High-Temperature Structures Tunnel (8' HTST) were investigated in a study of concepts to improve nozzle throat life and tunnel performance. The Langley 8' HTST provides realistic temperature simulation of Mach 7 hypersonic flight at altitudes of 24 to 40 km. The products of methane-air combustion are used as the test medium, and the combustion products are accelerated through the nozzle throat to produce hypersonic flow in the test section. During tunnel start-up and shut-down the nozzle throat is subjected to severe temperature changes. The severe thermal environment causes cracking in metallic nozzle throats and led to the consideration of ceramic nozzle insert concepts.

The nozzle throat insert problem serves as a convenient and demanding practical application for the evaluation of the integrated thermal-structural analysis approach. In Ref. 17, axisymmetric finite element thermal-structural models were employed, and the finite element model of the nozzle insert shown in Fig. 7a consisted of 117 solid elements. The analysis showed that temperature gradients in the axial direction are relatively mild, but the temperature gradients in the radial direction are severe. Herein, three-dimensional conventional and one-dimensional integrated axisymmetric element models (Fig. 7b) are employed to represent the radial thermal-structural behavior of the nozzle insert. A radial variation in the element size is used to better represent the thermal-structural response near the inner surface. The mesh spacing is the same as used in Ref. 17 and is identical for both conventional and integrated models. Temperature dependent thermal properties were considered in Ref. 17, but herein thermal properties are assumed constant. Plane strain (axial displacements equal to zero) is assumed for the structural analysis.

A detailed description of five nozzle presssure and thermal load cases is presented in Ref. 17. Herein, only one thermal load case is considered, and a simplified representation of the heating and cooling from the flowing gas stream is employed. The nozzle heating is represented as a convective boundary condition with time dependent properties:

$$T_\infty(t) = T_\infty \qquad 0 < t < 125 \text{ s}$$

$$= 0.2\, T_\infty \qquad 125 < t < 150 \text{ s}$$

$$h(t) = h_\infty \qquad 0 < t < 125 \text{ s}$$

$$= 0.1\, h_\infty \qquad 125 < t < 150 \text{ s}$$

This representation assumes an instantaneous rise and fall of the heating during tunnel combustion start-up at t = 0 and combustion shut-down at t = 125s. Temperature histories computed by the nodeless variable approach for five radial locations on the nozzle insert are shown in Fig. 8. These histories show that initially the temperature of the heated surface (point 1) rapidly approaches the convective exchange temperature, maintains nearly a constant value until 125 s and then declines rapidly as the nozzle is cooled by flow at the lower gas temperature. Temperatures in a thin layer near the surface tend to follow this trend also, but the outer surface (point 5) shows no change. Radial temperature variations at t = 1 s and t = 126 s are shown in Fig. 9a. These variations show the very sharp radial temperature gradients at early and late times in the response, and that the variations are confined to the inner region of the insert. The corresponding variation of the circumferential (hoop) stress is shown in Fig. 9b. The initial high temperature on the inner surface causes a sharply varying compressive stress in the inner region. As the temperature of the surface is reduced after 125 s, the inner surface stress drops significantly but the inner region maintains significant compressive stresses due to high internal temperatures. The portion of the nozzle outside of this region experiences a relatively small tensile stress throughout the response.

Temperature distributions computed by integrated elements, conventional elements and an exact analytical solution[19] are compared at t = 1 s in Fig. 10a. For the conventional finite element model, temperatures are computed for consistent and lumped capacitance matrices. The temperatures computed by the nodeless variable integrated element show the best agreement with the exact solution. The conventional elements with lumped capacitance predict temperatures that are too high, and the straight line interpolation gives a poor approximation to the exact distribution. The conventional elements with a consistent capacitance matrix predict temperatures for r/b = 0.575 that unrealistically oscillate below and above (not shown) the initial uniform cylinder temperature. An interpretation[20] of this unrealistic behavior is that the oscillations are an indication of the need for mesh refinement. However, the results show that although the mesh of conventional elements is inadequate to accurately represent the temperature distribution at this time, the nodeless variable integrated elements give good to excellent results with the same mesh.

Displacement and stress variations from the integrated and conventional finite element models

are compared with an exact solution[12] in Figs. 10b and 10c, respectively. Displacements computed from the integrated finite element approach show excellent agreement with the exact solution, but the conventional approach predicts displacements that are consistently too large. Stresses computed from the integrated elements also show excellent agreement with the exact stress solution, but the conventional elements also predict the stresses well, particularly the maximum stress which occurs on the inner surface. The reason that all methods show such good agreement is that the maximum stress at early response times is controlled by the temperature of the inner surface not the interior temperature distribution. In fact, for early response times, the maximum stress can be calculated[21] with good accuracy by

$$\sigma_\theta(a,t) = \frac{\alpha E}{1-\nu} [T(a,t) - T_r] \qquad (19)$$

where T_r is the initial uniform temperature.

Temperature and stress distributions computed by integrated and conventional elements are compared at t = 126 s in Figs. 11a and 11b, respectively. The figures show that the mesh is not sufficiently refined for the conventional elements to accurately represent the large variation of temperature and stress which occurs near the inner surface. The highly nonlinear variation of temperature and stress in this region cannot be realistically represented by the conventional element linear interpolation functions. The sharp discontinuities of the slopes of the temperature and stress curves at r/b = 0.575 are an indication of the inadequacy of the conventional element mesh. The integrated elements, however, predict realistic variation of the temperatures and stresses with good continuity of slopes of the temperature and stress curves. In comparison to the integrated analysis, the conventional approach with lumped capacitance underestimates the maximum temperature by 5 percent and underestimates the maximum stress by 9 percent and predicts the wrong locations for these maximums.

The examples demonstrate the potential of the integrated approach for the one dimensional examples considered. However, evaluation of the full potential of the approach requires additional investigation by: (1) applications to more complex structures with other finite elements, (2) consideration of nonlinear problems due to temperature dependent material properties, and (3) consideration of other heat transfer modes including radiation.

Concluding Remarks

An integrated transient thermal-structural finite element analysis approach is presented. The integrated thermal-structural analysis is characterized by: (1) thermal and structural finite elements formulated with a common geometric discretization with each element formulated to suit the needs of its respective analysis, (2) thermal and structural finite elements fully compatible during the coupling of the two analyses, and (3) use of equivalent thermal forces based on a consistent finite element formulation.

Integrated thermal-structural rod and one dimensional axisymmetric elements are developed and used to demonstrate the integrated analysis approach for conduction with surface convection. A unique feature of the elements is the use of nodeless variable interpolation functions for element temperatures and displacements. For steady-state linear analysis, the elements produce exact values of temperatures, displacements and stresses. This feature means the transient response can start from an exact initial temperature distribution, or if the response approaches thermal equilibrium for large time, exact steady-state temperatures, displacements and stresses are predicted.

The integrated thermal structural elements are evaluated by solving three transient examples of increasing complexity: (1) a rod with surface convection, (2) a cylinder with internal heating, and (3) a wind tunnel ceramic nozzle insert. Temperatures, displacements and stresses predicted by the integrated approach are compared with results from conventional finite elements and exact analytical solutions. In the examples, the integrated approach showed a clear superiority to the conventional finite element approach. For the same number of elements, the integrated approach has superior accuracy. For equivalent accuracy, fewer integrated elements are required; for instance, in the analysis of the cylinder with internal heating, two integrated elements gave results equivalent to predictions from twenty conventional elements. The nonlinear variation of temperatures, displacements and stresses within the integrated elements permits an accurate representation of these distributions with only a few elements. This feature was clearly demonstrated in the nozzle insert example which experienced sharp radial variations of the temperature and stresses due to instantaneous application and removal of convective heating. The examples demonstrate the approach offers significant potential and should be investigated further by applications of other element types to more complex thermal-structural problems.

References

1. Kelly, H. Neale, Rummler, Donald R. and Jackson, Robert L.: Research in Structures and Materials for Future Space Transportation Systems-An Overview. Presented at the AIAA Conference on Advanced Technology for Future Space Systems, May 8-11, 1979, Langley Research Center, Hampton, Virginia, AIAA Paper No. 79-0859.
2. Wieting, Allan R.: Application of Numerical Methods to Heat Transfer and Thermal Stress Analysis of Aerospace Vehicles, Numerical Methods in Thermal Problems, Proceedings of the First International Conference held at University College, Swansea, Wales, July 2-6, 1979, Pineridge Press, pp 634-643.
3. Adelman, Howard M., Sawyer, Patricia L. and Shore, Charles P.: Optimum Design of Structures at Elevated Temperatures, AIAA Journal, Vol. 17, Number 6, June 1979, pp. 622-629.
4. Thornton, Earl A. and Wieting, Allan R.: Evaluation of Finite-Element Formulations for Transient Conduction Forced-Convection

Analysis. Numerical Heat Transfer, Vol. 3, pp. 281-295, 1980.
5. Thornton, Earl A., Dechaumphai, Pramote and Wieting, Allan R.: Integrated Thermal-Structural Finite Element Analysis. Proceedings of the AIAA/ASME/ASCE/AHS 21st Structures, Structural Dynamics and Materials Conference, May 12-14, 1980. Seattle, Washington, pp. 957-969, AIAA Paper No. 80-0717.
6. Zienkiewiez, O. C., The Finite Element Method, third edition, McGraw-Hill Book Company, 1977.
7. Lee, H. P.: Application of Finite-Element Method in the Computation of Temperature with Emphasis on Radiative Exchanges, AIAA 7th Thermophysics Conference, San Antonio, Texas, April 10-12, 1972, AIAA Paper No. 72-274.
8. Lee, H. P., NASTRAN Thermal Analyzer, Vol. I: The NASTRAN Thermal Analyzer Manual, NASA Goddard Space Flight Center, X-322-76-16, Dec. 1975.
9. Christie, I., Griffiths, D. F. and Mitchell, A. R.: Finite Element Methods for Second Order Differential Equations with Significant First Derivatives, International Journal for Numerical Methods in Engineering, Vol. 10, 1976, pp. 1389-1396.
10. Huebner, K. H.: The Finite Element Method for Engineers, John Wiley and Sons, Inc., 1975, pp. 123-124.
11. Carslaw, H. S. and Jaeger, J. C.: Conduction of Heat in Solids, second edition, Oxford University Press, 1959, p. 327.
12. Boley, B. A. and Weiner, J. H.: Theory of Thermal Stress, John Wiley, 1960, pp. 288-291.
13. Thornton, Earl A.: TAP2: A Finite Element Program for Thermal Analysis of Convectively Cooled Structures, NASA CR-159038, Old Dominion University Research Foundation, 1980.
14. Bathe, K. J. and Wilson, E. L.: Numerical Methods in Finite Element Analysis, Prentice-Hall, 1976.
15. Whetstone, W. D.: SPAR Structural Analysis System Reference Manual Level 13A, Vol. 1: Program Execution. NASA CR-158970-1, 1978.
16. Marlowe, M. B.; Moore, R. A. and Whetstone, W. D.: SPAR Thermal Analysis Processors Reference Manual, System Level 16. NASA CR-159162, 1979.
17. Singh, J. P., Thomas, J. R., Jr., and Hasselman, D. P. H.: Stresses Due to Thermal Trapping in Semi-Absorbing Materials Subjected to Intense Radiation. Thermal Stresses in Severe Environments, edited by D. P. H. Hasselman and R. A. Heller, Plenum Press, New York, 1980, pp. 157-168.
18. Robinson, J. C., Smith, D. M., Puster, R. L. and Karns, J. R.: Analysis and Design of a Ceramic Nozzle Insert for the Langley 8-Foot High Temperature Structures Tunnel. Presented at 2nd Army-Navy-NASA-Air Force (JANNAF) Carbon-Carbon Nozzle Technology Meeting, Naval Postgraduate School, Monterey, CA. October 22-23, 1980.
19. Tauchert, T. R.: Thermal Stresses in Coal Conversion Pressure Vessels of Layered Construction. Thermal Stresses in Severe Environments, edited by D. P. H. Hasselman and R. A. Heller, Plenum Press, New York, 1980, pp. 183-205.
20. Gresho, P. and Lee, R. L.: Don't Suppress the Wiggles--They're Telling You Something. ASME Symposium on Finite Element Methods for Convection Dominated Flows, ASME Winter Annual Meeting, New York, Dec. 1979.
21. Timoshenko, S. and Goodier, J. N.: Theory of Elasticity, McGraw-Hill, 1951.

Appendix A: Rod Element

The rod element matrices are derived from the general element equations (3) and (6) using the element temperature and displacement interpolation functions given in Tables 2 and 3, respectively.

Capacitance Matrices

$$C_{00} = \rho cAL/30$$
$$C_{01} = C_{02} = \rho cAL/12$$
$$C_{11} = C_{22} = \rho cAL/3$$
$$C_{12} = C_{21} = \rho cAL/6 \qquad \text{(Cases 1-3)}$$

$$C_{00} = \rho cA\left[\left(\frac{\cosh mL-1}{\sinh mL}\right)\left(\frac{L}{\sinh mL} - \frac{3}{m}\right) + L\right]$$
$$C_{01} = C_{02} = \rho cA\left[\frac{(1-\cosh mL)(mL-\sinh mL)}{2m\sinh^2 mL}\right]$$
$$C_{11} = C_{22} = \rho cA\left[\frac{\sinh mL \cosh mL - mL}{2m\sinh^2 mL}\right] \qquad \text{(Case 4)}$$
$$C_{12} = C_{21} = \rho cA\left[\frac{mL\cosh mL - \sinh mL}{2m\sinh^2 mL}\right]$$

where

$$m = \sqrt{hp/kA}$$

Conductance Matrices

$$K_{00} = kA/3L$$
$$K_{01} = K_{02} = 0$$
$$K_{11} = K_{22} = kA/L$$
$$K_{12} = K_{21} = -kA/L \qquad \text{(Cases 1-3)}$$

$$K_{00} = \frac{hp}{m}\left[mL - \frac{2(\cosh mL - 1)}{\sinh mL}\right]$$
$$K_{01} = K_{02} = 0$$
$$K_{11} = K_{22} = \frac{hp}{m}\left[\frac{\cosh mL}{\sinh mL}\right] \qquad \text{(Case 4)}$$
$$K_{12} = K_{21} = \frac{hp}{m}\left[-\frac{1}{\sinh mL}\right]$$

For case 4, the conductance matrix includes the contributions from conduction and convection given in equations (3b-3c).

Heat Load Vectors

$$\{Q\}^T = QAL\ [1/6 \quad 1/2 \quad 1/2] \qquad \text{(Case 2)}$$

$$\{Q\}^T = qpL\ [1/6 \quad 1/2 \quad 1/2] \quad \text{(Case 3)}$$

$$Q_0 = hpT_\infty\left[L - \frac{2}{m}\left(\frac{\cosh mL - 1}{\sinh mL}\right)\right] \quad \text{(Case 4)}$$

$$Q_1 = Q_2 = hpT_\infty\left[\frac{1}{m}\left(\frac{\cosh mL - 1}{\sinh mL}\right)\right]$$

Stiffness Matrix

$$K_{11} = K_{22} = AE/L$$

$$K_{12} = K_{21} = -AE/L \quad \text{(Cases 1-4)}$$

Force Vector

$$\{F\}^T = [-F \quad F]$$

where

$$F = \alpha EA[T_o/6 + (T_1 + T_2)/2] \quad \text{(Cases 1-3)}$$

$$F = \alpha EA[C_1T_o + C_2(T_1 + T_2)] \quad \text{(Case 4)}$$

and

$$C_1 = 1 - \frac{2\ (\cosh mL - 1)}{mL\ \sinh mL}$$

$$C_2 = \frac{\cosh mL - 1}{mL\ \sinh mL}$$

Appendix B: Axisymmetric Element

The axisymmetric element matrices are derived from the general element equation (3) and (6) using the element temperature and displacement interpolation functions given in Tables 4 and 5, respectively. Matrices are the same for all cases except where noted.

Capacitance Matrix

$$C_{00} = \rho c\left\{\frac{b^2-a^2}{24\ b^4}\left[4w^2(a^4+a^2b^2+b^4) + 9w(a^4-b^4) + 6(a^2-b^2)^2\right]\right\}$$

$$C_{01} = -\frac{\rho c}{16b^2w}\left[4a^4w^2+w(7a^2+3b^2)(a^2-b^2) + 4(a^2-b^2)^2\right]$$

$$C_{02} = \frac{\rho c}{16b^2w}\left[4b^4w^2 - w\ (7b^2+3a^2)(b^2-a^2) + 4(a^2-b^2)^2\right]$$

$$C_{11} = \frac{\rho c}{4w^2}\left[b^2 - a^2\ (1 + 2w + 2w^2)\right]$$

$$C_{12} = C_{21} = \frac{\rho c}{4w^2}\left[a^2 - b^2 + w(a^2 + b^2)\right]$$

$$C_{22} = \frac{\rho c}{4w^2}\left[b^2\ (1 - 2w + 2w^2) - a^2\right]$$

where $w = \ln(b/a)$.

Conductance Matrix

$$K_{00} = kw\left[w\left(1-(a/b)^4\right) - \left(1-(a/b)^2\right)^2\right]$$

$$K_{01} = K_{02} = 0$$

$$K_{11} = K_{22} = k/w$$

$$K_{12} = K_{21} = -k/w$$

For surface convection on the cylinder inner and outer surfaces additional conductances are added to the system conductance matrix:

$$r = a, \quad K_h = ha$$

$$r = b, \quad K_h = hb$$

Heat Load Vectors

$$Q_0 = \frac{Qb^2}{4w}\left[w^2\ (1 - \frac{a^4}{b^4}) - w\ (1 - \frac{a^2}{b^2})^2\right]$$

$$Q_1 = \frac{Q}{w}\left[-\frac{a^2}{2}w + \frac{1}{4}(b^2 - a^2)\right]$$

$$Q_2 = \frac{Q}{w}\left[\frac{b^2}{2}w - \frac{1}{4}(b^2 - a^2)\right] \quad \text{(Case 2)}$$

For the surface convection and surface heating on the cylinder inner and outer surfaces additional nodal heat loads are added to the system heat load vector:

$$r = a, \quad Q = haT_\infty + qa$$

$$r = b, \quad Q = hbT_\infty + qb$$

Stiffness Matrix (Plane stress)

$$K_{11} = \frac{E}{(1-\nu^2)}\frac{1}{(b^2-a^2)}\left[(b^2 + a^2) - \nu(b^2 - a^2)\right]$$

$$K_{12} = \frac{E}{(1-\nu^2)}\frac{1}{(b^2-a^2)}\left[-2ab\right]$$

$$K_{22} = \frac{E}{(1-\nu^2)}\frac{1}{(b^2-a^2)}\left[(b^2 + a^2) + \nu(b^2 - a^2)\right]$$

Force Vector (Plane stress)

$$F_1 = \frac{E\alpha}{(1-\nu)}\frac{1}{w(b^2-a^2)}\left\{-\frac{a}{2}\left[(-2a^2w+b^2-a^2)(T_1+\frac{a^2}{b^2}wT_o) + (2b^2w-b^2+a^2)(T_2+wT_o) - \frac{b^4-a^4}{b^2}w^2\ T_o - 2(b^2-a^2)w\ T_r\right]\right\}$$

$$F_2 = \frac{E\alpha}{(1-\nu)}\frac{1}{w(b^2-a^2)}\left\{\frac{b}{2}\left[(-2a^2w+b^2-a^2)(T_1+\frac{a^2}{b^2}wT_o) + (2b^2w-b^2+a^2)(T_2+wT_o) - \frac{b^4-a^4}{b^2}w^2\ T_o - 2(b^2-a^2)w\ T_r\right]\right\}$$

Table 1 Rod Element Heat Transfer Cases

CASE	HEAT TRANSFER MODE
1	CONDUCTION WITH NO HEATING
2	CONDUCTION WITH INTERNAL HEAT GENERATION
3	CONDUCTION WITH SURFACE HEAT FLUX
4	CONDUCTION WITH SURFACE CONVECTION

Table 2 Rod Element Interpolation Functions

Case	Nodeless Parameter, T_0	$N_0(x)$	$N_1(x)$	$N_2(x)$
1	0	$\frac{x}{L}\left(1-\frac{x}{L}\right)$	$1-\frac{x}{L}$	$\frac{x}{L}$
2	$\frac{QL^2}{2k}$	$\frac{x}{L}\left(1-\frac{x}{L}\right)$	$1-\frac{x}{L}$	$\frac{x}{L}$
3	$\frac{qpL^2}{2kA}$	$\frac{x}{L}\left(1-\frac{x}{L}\right)$	$1-\frac{x}{L}$	$\frac{x}{L}$
4	T_∞	$1-\frac{\sinh m(L-x)}{\sinh mL}-\frac{\sinh mx}{\sinh mL}$	$\frac{\sinh m(L-x)}{\sinh mL}$	$\frac{\sinh mx}{\sinh mL}$

WHERE $m=\sqrt{\frac{hp}{kA}}$

Table 3 Rod Element Displacement Interpolation Functions, $N_S(X)$*

CASE	$N_0(X)$
1	$\frac{\alpha(T_2-T_1)L}{2}(X^2-X)$
2	$\frac{\alpha(T_2-T_1)L}{2}(X^2-X)+\frac{\alpha T_0 L}{6}(-X+3X^2-2X^3)$
3	$\frac{\alpha(T_2-T_1)L}{2}(X^2-X)+\frac{\alpha T_0 L}{6}(-X+3X^2-2X^3)$
4	$\alpha\left\{\frac{T_2-T_1\cosh mL+T_0(\cosh mL-1)}{m\sinh mL}\left[(\cosh mLX-1)-X(\cosh mL-1)\right]+\frac{T_1-T_0}{m}(\sinh mLX-X\sinh mL)\right\}$

*For all cases, $N_1(X)=1-X$ $N_2(X)=X$

Table 4 Axisymmetric Element Temperature Interpolation Functions

Case	Nodeless Parameter, T_o
1	0
2	$Qb^2/(4kw)$

$$N_o(r) = \ln(r/a) + a^2\ln(b/r)/b^2 - r^2w/b^2$$

$$N_1(r) = \ln(b/r)/w$$

$$N_2(r) = \ln(r/a)/w$$

where $w = \ln(b/a)$

Table 5 Axisymmetric Element Displacement Interpolation Functions

$$N_o(r) = \frac{\alpha(1+\nu)}{2rw}\left\{(T_1+\frac{a^2}{b^2}wT_o)\left[r^2\ln(\frac{b}{r})-\frac{(b^2-r^2)a^2w}{(b^2-a^2)}\right]\right.$$

$$+(T_2+wT_o)\left[r^2\ln(\frac{r}{a})-\frac{(r^2-a^2)b^2w}{(b^2-a^2)}\right]$$

$$\left.+\ w^2T_o\left[\frac{(b^2-r^2)(r^2-a^2)}{2b^2}\right]\right\}$$

$$N_1(r) = \frac{a(b^2-r^2)}{r(b^2-a^2)}$$

$$N_2(r) = \frac{b(r^2-a^2)}{r(b^2-a^2)}$$

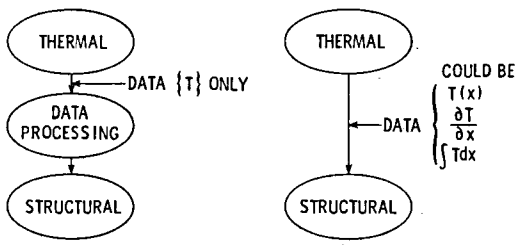

(a) Conventional analysis. (b) Integrated analysis.

Fig. 1 Conventional versus integrated thermal and structural analysis.

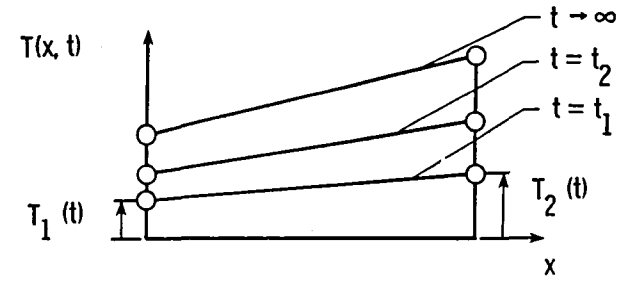

(a) Conventional.

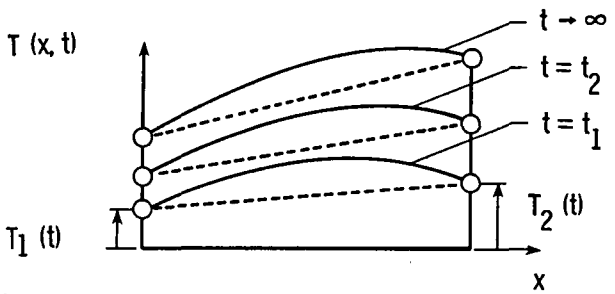

(b) Nodeless parameter.

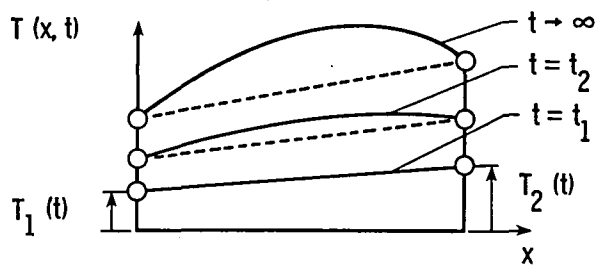

(c) Nodeless variable.

Fig. 2 One dimensional element interpolation functions.

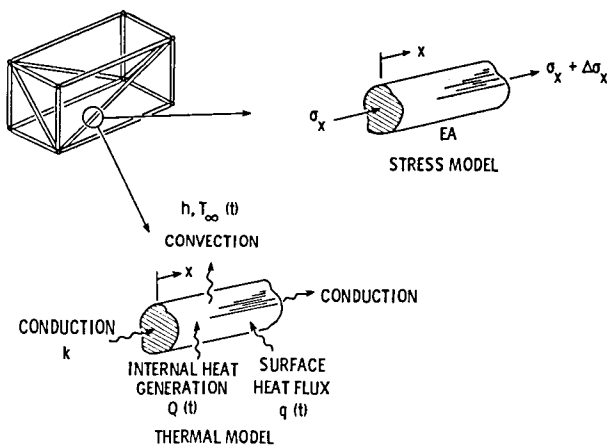

Fig. 3 Thermal and stress models of rod element.

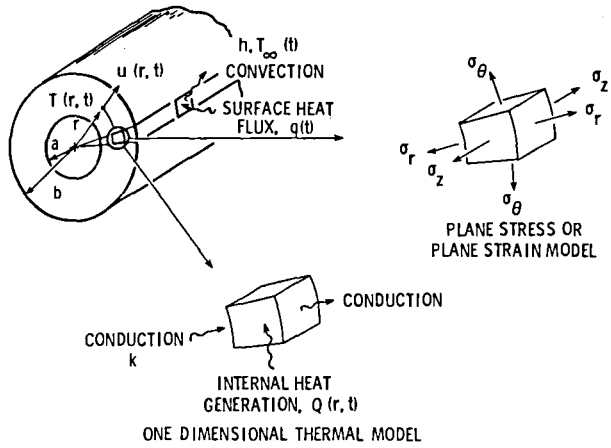

Fig. 4 Thermal and stress models of axisymmetric element.

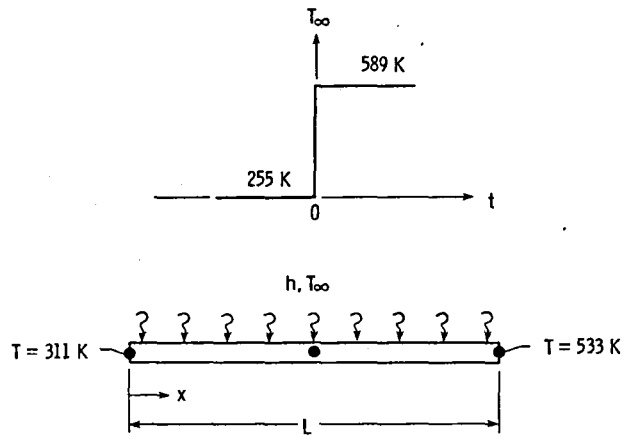

(a) Rod heated by surface convection.

Fig. 5 Conventional and integrated finite element solutions for a rod with surface convection.

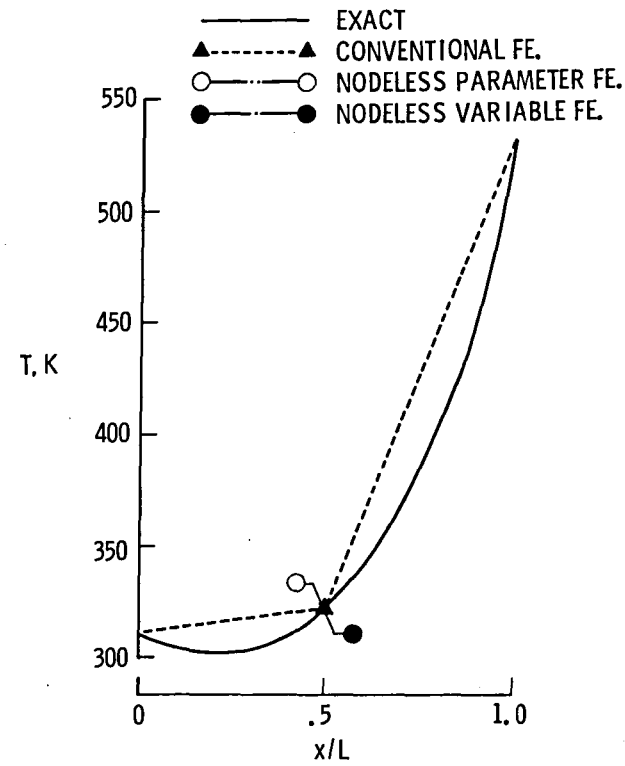

(b) Comparative temperature distributions at t = 0s.

Fig. 5 Continued.

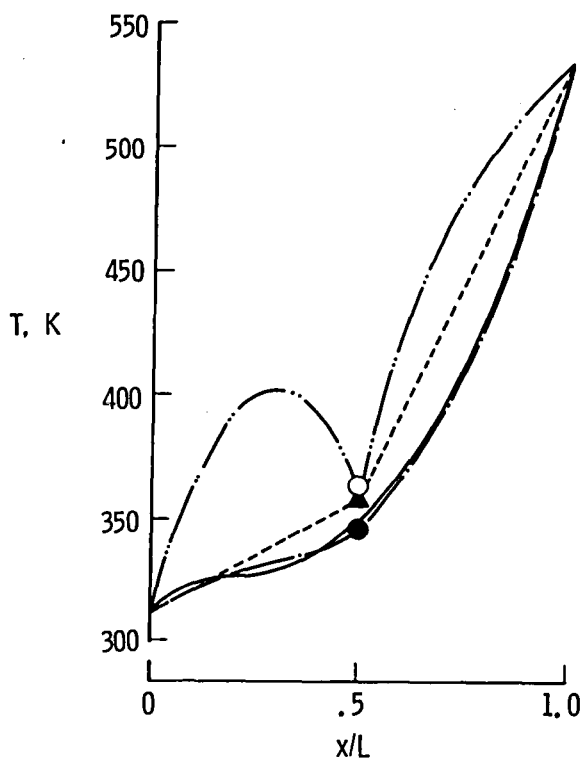

(c) Comparative temperature distributions at t = .01s.

Fig. 5 Continued.

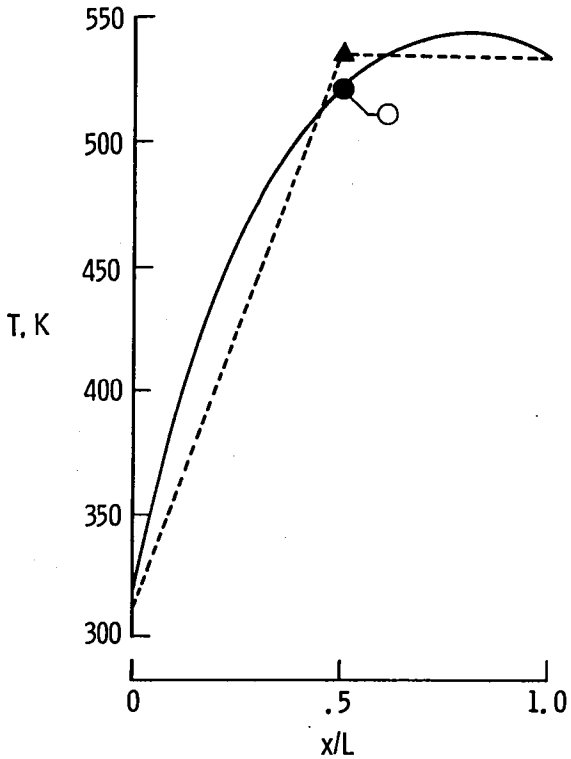

(d) Comparative temperature distributions at t = .30s.

Fig. 5 Concluded.

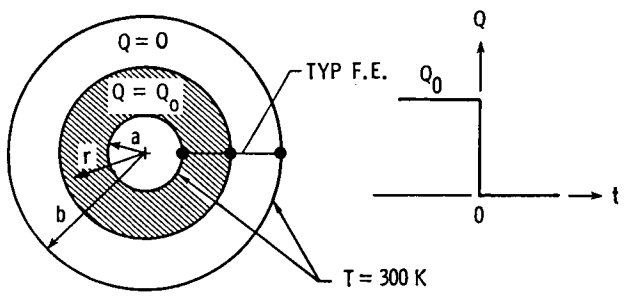

(a) Cylinder with internal heat generation.

Fig. 6 Conventional and integrated finite element solutions for cylinder with internal heating.

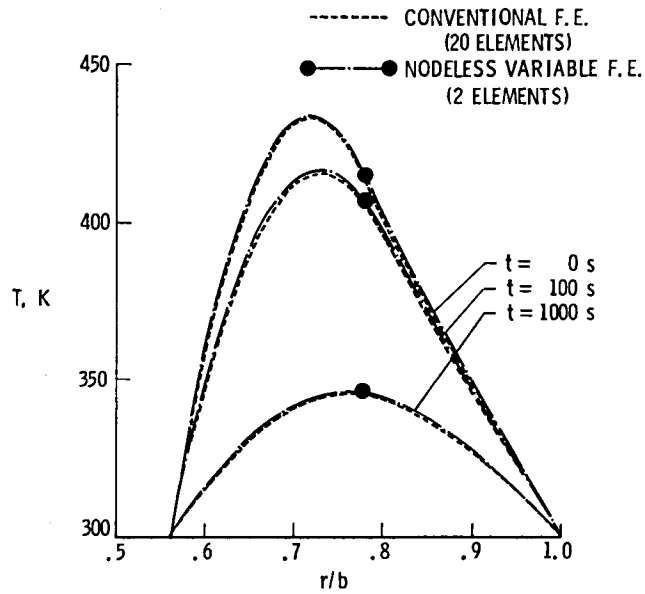

(b) Comparative temperature distributions.

Fig. 6 Continued.

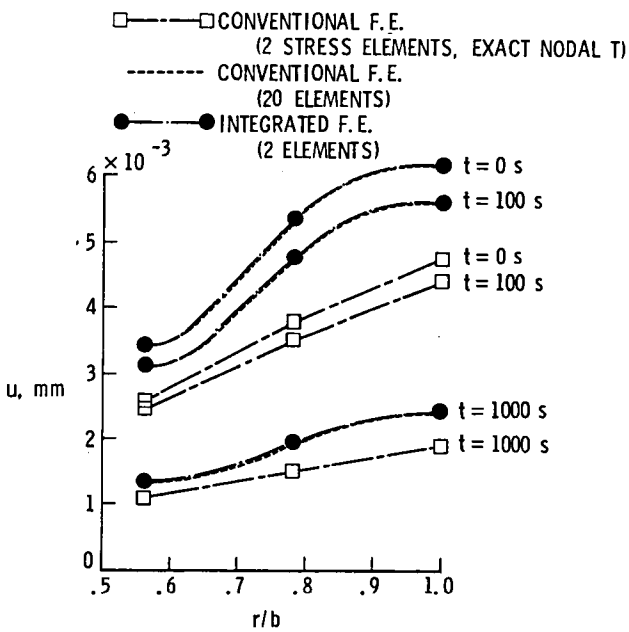

(c) Comparative displacement distributions.

Fig. 6 Continued.

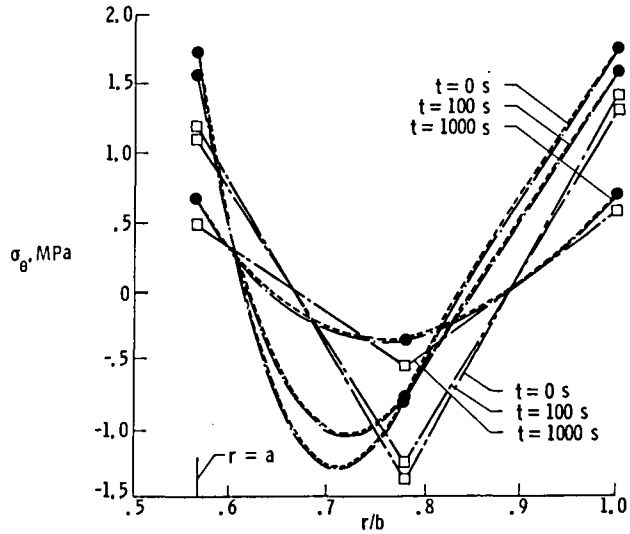

(d) Comparative circumferential stress distributions.

Fig. 6 Concluded.

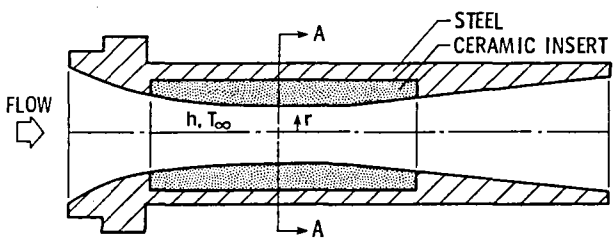

(a) Nozzle cross section.

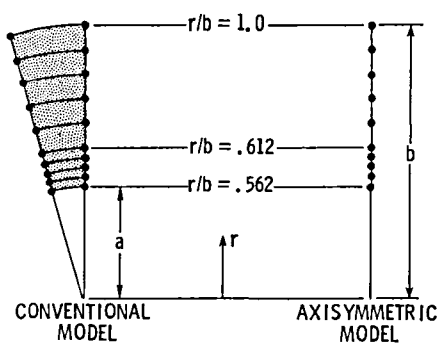

(b) Finite element models at section A-A.

Fig. 7 Tunnel nozzle insert and thermal-structural models.

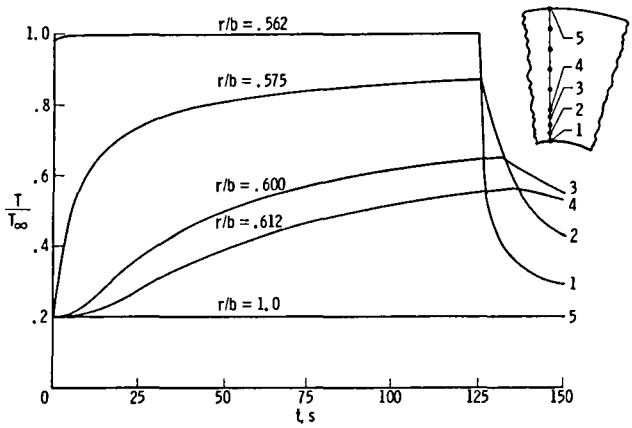

Fig. 8 Nozzle insert temperature response computed by nodeless variable finite elements.

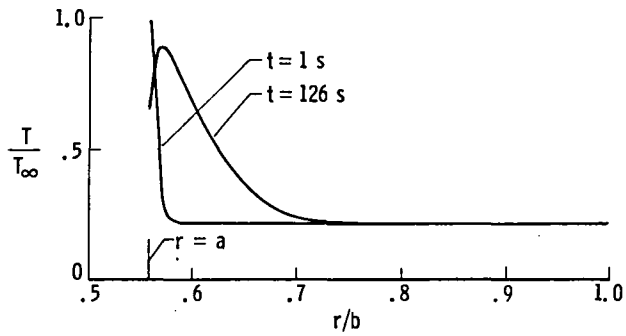

(a) Nozzle temperature distributions.

Fig. 9 Nozzle insert temperature and stress distribution computed by integrated thermal-structural finite elements.

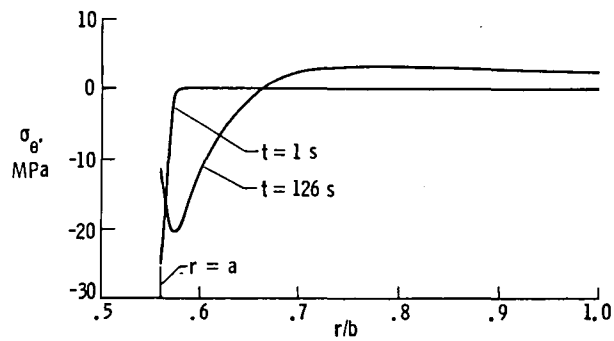

(b) Nozzle circumferential stress distributions.

Fig. 9 Concluded.

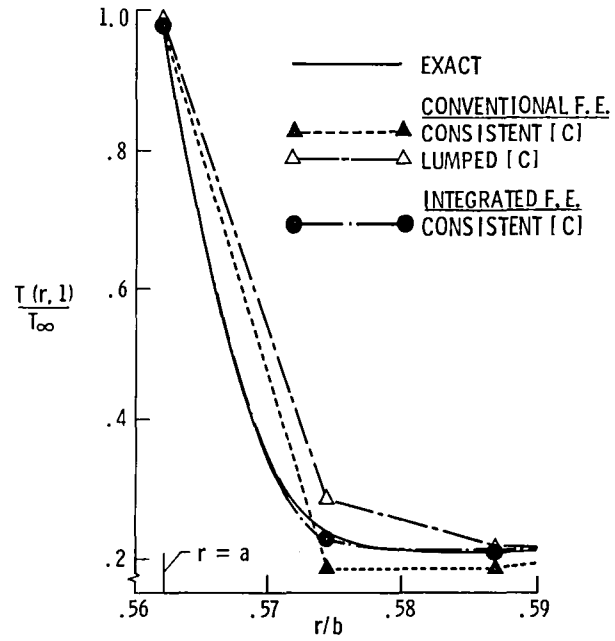

(a) Comparative temperature distributions.

Fig. 10 Comparison of nozzle temperatures, stresses and displacements at t = 1s.

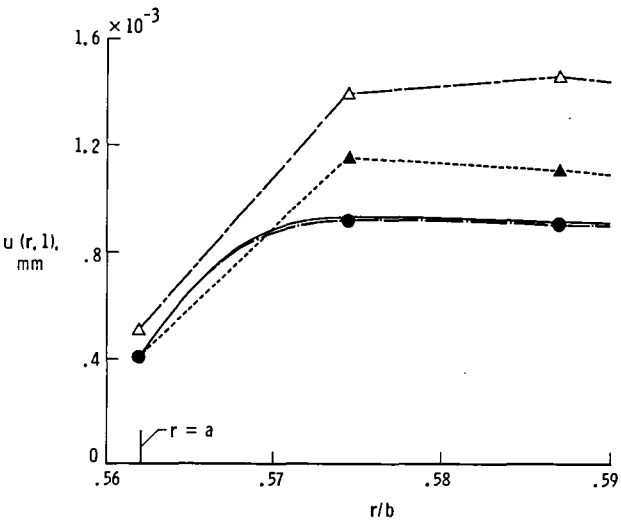

(b) Comparative displacement distributions.

Fig. 10 Continued.

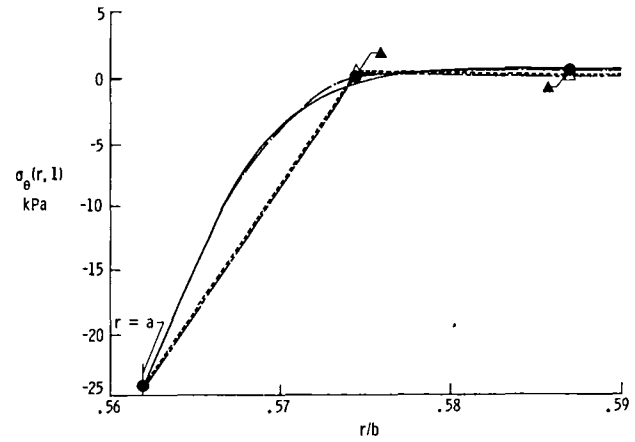

(c) Comparative circumferential stress distributions.

Fig. 10 Concluded.

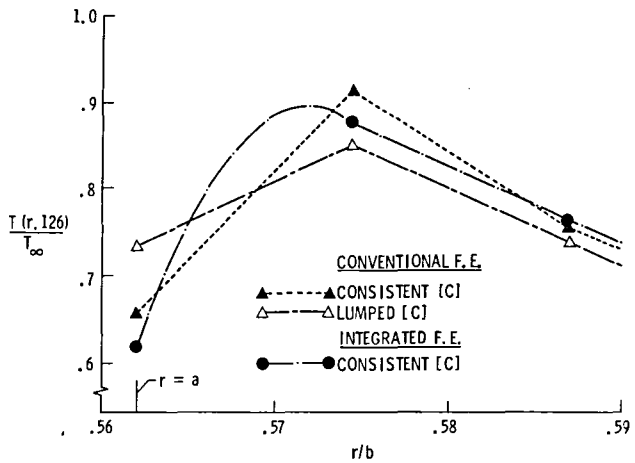

(a) Comparative temperature distributions.

Fig. 11 Comparison of nozzle temperatures and stresses at t = 126s.

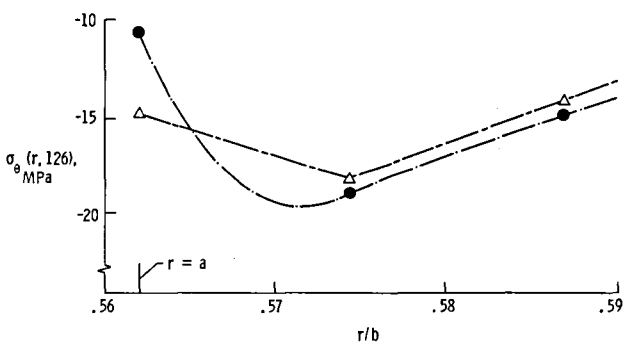

(b) Comparative circumferential stress distributions.

Fig. 11 Concluded.

1. Report No.	2. Government Accession No.	3. Recipient's Catalog No.
NASA TM-83125		

4. Title and Subtitle	5. Report Date
Integrated Transient Thermal-Structural Finite Element Analysis	May 1981
	6. Performing Organization Code 506-53-33-04

7. Author(s)	8. Performing Organization Report No.
Earl A. Thornton*, Pramote Dechaumphai*, Allan R. Wieting**, and Kumar K. Tamma*	
	10. Work Unit No.

9. Performing Organization Name and Address	11. Contract or Grant No.
NASA Langley Research Center Hampton, VA 23665	

12. Sponsoring Agency Name and Address	13. Type of Report and Period Covered
National Aeronautics and Space Administration Washington, DC 20546	Technical Memorandum
	14. Sponsoring Agency Code

15. Supplementary Notes

This paper was presented at the AIAA Structural Dynamics Specialists Meeting, April 9-10, 1981, Atlanta, Georgia
*Old Dominion University, Norfolk, VA; **NASA Langley Research Center, Hampton, VA

16. Abstract

An integrated thermal-structural finite element approach for efficient coupling of transient thermal and structural analysis is presented. New integrated thermal-structural rod and one dimensional axisymmetric elements considering conduction and convection are developed and used in transient thermal-structural applications. The improved accuracy of the integrated approach is illustrated by comparisons with exact transient heat conduction-elasticity solutions and conventional finite element thermal-finite element structural analyses. Results indicate that the approach offers significant potential for further development with other elements.

17. Key Words (Suggested by Author(s))	18. Distribution Statement
Heat Transfer Integrated Thermal Structural Analysis Finite Element Analysis	Unclassified - Unlimited Subject Category 34

19. Security Classif. (of this report)	20. Security Classif. (of this page)	21. No. of Pages	22. Price
Unclassified	Unclassified	17	A02

End of Document